Spatiotemporal Variations of Extreme Precipitation in the Guanzhong Plain and Their Relationship with Atmospheric Circulation (Postprint)

Authors: Ding Yingying

Date: 2022-01-26T18:02:44+00:00

Abstract

Based on daily precipitation data from 13 meteorological stations in the Guanzhong Plain from 1957 to 2019, various extreme precipitation indices were calculated using methods such as simple linear regression, Pearson correlation analysis, and wavelet coherence analysis, and their spatiotemporal variation characteristics were analyzed to explore the relationship between extreme precipitation and atmospheric circulation. The results show that: (1) Temporally, except for the extreme precipitation intensity which increased at a rate of 0.007 mm · d-1 · (10a)-1, all other extreme precipitation indices showed a decreasing trend, among which the annual total extreme precipitation (PRCPTOT) decreased the fastest, with a decreasing rate of -5.528 mm · (10a)-1, and none of the extreme precipitation indices had significant abrupt change points. (2) Spatially, extreme precipitation indices were higher in the south and lower in the north, with significant spatial differences. (3) The Southern Oscillation Index (SOI), which reflects atmospheric circulation, had the most significant impact on extreme precipitation. The larger the SOI, the more likely the Guanzhong Plain is to experience low precipitation. This study can provide a scientific theoretical basis for flood disaster prevention and control in the Guanzhong Plain.

Full Text

Spatial-temporal Variations in Extreme Precipitation and Their Relationship with Atmospheric Circulation in the Guanzhong Plain

DING Yingying[1], QIU Dexun[2], WU Changxue[1], MU Xingmin[1,2], GAO Peng[1,2]

[1]State Key Laboratory of Soil Erosion and Dryland Farming on the Loess Plateau, Institute of Soil and Water Conservation, Northwest A&F University, Yangling 712100, Shaanxi, China
[2]Institute of Soil and Water Conservation, Chinese Academy of Sciences and Ministry of Water Resources, Yangling 712100, Shaanxi, China

Abstract

Based on daily precipitation data from 13 meteorological stations in the Guanzhong Plain, we calculated various extreme precipitation indices and analyzed their spatiotemporal variation characteristics using unitary linear regression, Pearson correlation analysis, and wavelet coherence analysis. The relationship between extreme precipitation and atmospheric general circulation was also explored. The results revealed three key findings. First, extreme precipitation intensity exhibited an increasing trend at a rate of 0.007 mm $\cdot$ $d^{-1} \cdot (10a)^{-1}$, while other extreme precipitation indices showed decreasing trends. Among these, the annual total extreme precipitation (PRCPTOT) decreased most rapidly at a rate of -5.528 mm $\cdot$ $(10a)^{-1}$, and none of the indices exhibited significant mutation points. Second, spatially, all extreme precipitation indices displayed a pattern of higher values in the south and lower values in the north, with pronounced spatial heterogeneity. Third, among the atmospheric circulation factors examined, the Southern Oscillation Index (SOI) exerted the most significant influence on extreme precipitation; higher SOI values were associated with drier conditions in the Guanzhong Plain. These findings provide a scientific theoretical basis for flood disaster prevention and water resources management in the region.

Keywords: Guanzhong Plain; extreme precipitation; spatial-temporal variation; atmospheric circulation

Introduction

The water cycle constitutes a fundamental material circulation process connecting oceans and inland areas for water resource renewal, with precipitation representing a critical component of this cycle. Under the influence of global climate change and intensifying human activities, the water cycle has accelerated, leading to frequent extreme precipitation events. Although these events are statistically low-probability occurrences, they exhibit strong uncertainty in duration and often cause catastrophic damage when persisting for multiple days, frequently triggering geological disasters such as flash floods, debris flows, and landslides that threaten lives and property.

The Guanzhong Plain, encircled by the Qinling Mountains to the south and the Northern Shaanxi Plateau, possesses a unique geographical setting that obstructs moisture transport and alters regional water cycle processes. Numerical simulation studies have demonstrated that precipitation in the eastern part of the plain is lower than in the western part, likely due to the blocking effect

of the Qinling Mountains. The region is also influenced by the subtropical high-pressure system, which prevents warm, moist air from reaching northern Eurasia through monsoon circulation, resulting in reduced winter and spring precipitation. Atmospheric circulation anomalies represent the direct cause of climate variability, and the increasing frequency of extreme precipitation events is closely related to such anomalies. Variations in sea-level pressure between the eastern and western Pacific affect wind patterns, atmospheric circulation, and moisture transport, thereby influencing precipitation processes. The Southern Oscillation Index (SOI), which reflects large-scale atmospheric circulation, is intimately connected with El Niño phenomena. Previous research has shown that when SOI strengthens, precipitation in the Guanzhong region decreases.

Current research on extreme precipitation primarily focuses on spatiotemporal variation patterns, relationships with atmospheric circulation, event simulation, and future predictions based on artificial neural networks and machine learning. Studies have covered regions including South China, Southwest China, and major river basins. For instance, analysis of daily precipitation data in South China from 1959 to 2016 revealed that large-scale atmospheric circulation significantly influences extreme precipitation in the region. In the Weihe River Basin, comparative analysis of upper, middle, and lower reaches indicated substantial interannual precipitation variation after 1990, with more pronounced changes in the middle reaches. As the alluvial plain of the Weihe River located in the middle reaches, the Guanzhong Plain is sensitive to climate change. Moreover, recent decades have witnessed an increasing trend of heavy precipitation events in Northwest China. However, the underlying mechanisms through which atmospheric circulation influences extreme precipitation in this region remain unclear, necessitating further investigation to provide theoretical support for water resources allocation, agricultural and industrial development, and flood disaster prevention in the Guanzhong Plain.

2.1 Data Sources

Daily precipitation data from 13 meteorological stations in the Guanzhong Plain were obtained from the China Meteorological Data Sharing Service Network. Missing data were interpolated using neighboring stations, and the RClimDex software was employed for quality control and consistency checking, with all datasets demonstrating good performance. The digital elevation model (DEM) data for the Guanzhong Plain were derived from the Geospatial Data Cloud platform and the 30-meter resolution DEM product jointly measured by NASA and the National Imagery and Mapping Agency. Indices reflecting atmospheric circulation, including the Southern Oscillation Index (SOI), Atlantic Multidecadal Oscillation (AMO), North Atlantic Oscillation (NAO), Arctic Oscillation (AO), North Pacific Teleconnection Pattern (NP), Pacific Decadal Oscillation (PDO), and Pacific Index (PI), were obtained from the Earth System Research Laboratory of the National Oceanic and Atmospheric Administration.

2.2.1 Selection of Extreme Precipitation Indices

Following the recommendations of the Expert Team on Climate Change Detection and Indices (ETCCDI) established by the World Meteorological Organization' s Commission for Climatology, and considering the climate type of the Guanzhong Plain, six extreme precipitation indices were selected. These indices reflect precipitation amount, precipitation days, and precipitation intensity in the study area (Table 1).

2.2.2 Unitary Linear Regression

Temporal variation trends of extreme precipitation indices were analyzed using the least squares method of linear regression and moving average techniques. The slope of the linear regression equation represents the linear tendency rate. A positive slope indicates an increasing trend, while a negative slope indicates a decreasing trend, with the absolute magnitude reflecting the rate of change. The non-parametric Mann-Kendall test was applied to assess the significance of trends in each extreme precipitation index, yielding Z-values that indicate the significance level. When the absolute Z-value exceeds the critical value at $\alpha = 0.05$ or $\alpha = 0.01$, the increasing or decreasing trend is considered statistically significant. The Mann-Kendall test was also used for mutation point detection by constructing UFk and UBk curves; intersection points within the critical lines indicate the onset of mutation.

2.2.3 Wavelet Coherence Analysis

Wavelet coherence analysis, derived from Fourier coherence, can intuitively reflect the phase relationship and local correlation between influencing factors and runoff through cross-wavelet coherence spectra. In the spectrum, the cone-shaped line region represents the effective spectral value area, thick solid lines denote confidence intervals passing the 0.05 significance level, and arrow directions indicate phase relationships between the two time series. Rightward arrows represent in-phase (positive correlation), leftward arrows represent anti-phase (negative correlation), downward arrows indicate the influencing factor leads runoff change (by 1/4 period), and upward arrows indicate it lags. The effective spectral value region avoids boundary effects and high-frequency false information. The cross-wavelet power between two time series X and Y is defined as the product of their continuous wavelet transforms, and wavelet coherence is calculated as the squared magnitude of the smoothed cross-wavelet spectrum normalized by the product of the smoothed individual wavelet power spectra. This method was employed to analyze the local correlation between extreme precipitation indices and atmospheric circulation factors.

3.1.1 Temporal Variation

Based on daily precipitation data from each meteorological station, the Thiessen polygon method was used to calculate regional extreme precipitation indices.

Analysis of their temporal trends over the past 63 years revealed that all extreme precipitation indices showed non-significant trends except for extreme precipitation intensity, which increased at a rate of 0.007 $mm \cdot d^{-1} \cdot (10a)^{-1}$. The other indices exhibited non-significant decreasing trends, with PRCPTOT decreasing most rapidly at -5.528 $mm \cdot (10a)^{-1}$. The moving average trend line showed recurrent patterns, with decreasing trends before the 1990s and a more pronounced increasing trend after 2000. PRCPTOT showed the greatest interannual variability, with a multi-year average of 513.36 mm, maximum of 783.45 mm, and minimum of 332.6 mm. RX1day and RX5day decreased at rates of -0.105 $mm \cdot (10a)^{-1}$ and -0.096 $mm \cdot (10a)^{-1}$, respectively. The consecutive wet days index (CWD) showed a non-significant decreasing trend at -0.171 $d \cdot (10a)^{-1}$ with large fluctuations, while R10mm decreased at -0.005 $d \cdot (10a)^{-1}$. Mann-Kendall mutation tests revealed no significant mutation points for any extreme precipitation indices.

3.1.2 Spatial Variation

Spatial distribution and variation trends of extreme precipitation indices were interpolated using the inverse distance weighting method based on multi-year averages and linear tendency rates from 13 stations. Spatially, extreme precipitation exhibited a clear pattern of higher values in the south and lower values in the north, with significant spatial heterogeneity. All indices decreased from the southwestern Foping station and southeastern areas toward the northwest. The maximum PRCPTOT occurred at Foping station (910.53 mm), while the minimum occurred at Kongtong station in the northwest (495.91 mm). R10mm showed a similar pattern, with maximum at Foping station (15.56 days) and minimum at Kongtong station (6.25 days). RX1day and RX5day also peaked at Foping station (50.76 mm and 81.35 mm, respectively) and reached minima at Kongtong station (27.57 mm and 69.2 mm, respectively). The maximum SDII occurred at Huashan station (10.25 $mm \cdot d^{-1}$).

In terms of spatial trends, 69.2% of stations showed decreasing PRCPTOT trends, with Zhengan station exhibiting the largest decrease (-18.7 $mm \cdot (10a)^{-1}$). For R10mm, 92.3% of stations showed decreasing trends, with Pucheng station showing the most significant decline (-0.47 $d \cdot (10a)^{-1}$). RX1day increased at Kongtong, Changwu, Foping, and Longxian stations, with Changwu showing the largest increase (1.2 $mm \cdot (10a)^{-1}$), while other stations showed decreasing trends. RX5day decreased at most stations except Kongtong, with Pucheng showing the most significant decrease (-4.48 $mm \cdot (10a)^{-1}$). SDII showed increasing trends across most of the plain except the southeast, with significant increases in the northwest.

3.2 Consistency Among Extreme Precipitation Indices

Significant positive correlations existed among all extreme precipitation indices except SDII, with correlation coefficients ranging from 0.29 to 0.80 (all passing the 0.01 significance level). PRCPTOT showed particularly strong correlations

with R10mm (0.73), RX1day (0.45), and RX5day (0.68), all significant at the 0.01 level. These relationships indicate that the selected extreme precipitation indices effectively represent total annual precipitation, with their increases or decreases reflecting corresponding changes in precipitation amount (Table 4).

3.3.2 Association Analysis Between Extreme Precipitation Indices and SOI

Wavelet coherence analysis was used to further explore the relationship between SOI and extreme precipitation indices at low-frequency scales. The analysis revealed significant negative correlations between SOI and PRCPTOT in the 2-4 year band, with a resonance period of 3-4 years and a phase difference of approximately 5-6 months. In the 4-5 year band, significant positive correlations emerged after 1990, with correlation coefficients reaching 0.8. R10mm showed significant positive correlations with SOI in the 4-5 year band, with a phase difference of about 4-5 months and local correlation coefficients up to 0.7. RX1day and RX5day exhibited similar patterns, with significant positive correlations in the 4-5 year band and phase differences of approximately 4-5 months. These results demonstrate that SOI is the most influential atmospheric circulation factor affecting extreme precipitation in the Guanzhong Plain, with higher SOI values associated with increased likelihood of dry conditions.

4 Conclusion

This study investigated the spatiotemporal variations of extreme precipitation indices and their relationship with atmospheric circulation in the Guanzhong Plain over the past 63 years. Three main conclusions were drawn. First, except for extreme precipitation intensity, which showed an increasing trend, all other indices exhibited non-significant decreasing trends, with PRCPTOT decreasing most rapidly at -5.528 $mm \cdot (10a)^{-1}$ and no significant mutation points detected. Second, spatially, extreme precipitation indices displayed a consistent pattern of higher values in the south and lower values in the north, with maximum values concentrated in the southeastern and southwestern regions, particularly at Foping station, while the northwestern region experienced more concentrated extreme precipitation events. Third, among the atmospheric circulation factors examined, SOI had the most significant impact on extreme precipitation, with higher SOI values correlating with drier conditions in the Guanzhong Plain. The wavelet coherence analysis revealed significant resonance periods of 4-5 years between SOI and extreme precipitation indices. These findings provide crucial scientific support for flood disaster prevention and water resources management in the Guanzhong Plain.

References

[1] Zhou Qi, Zhang Haining, Ren Yuanxin. A study on extreme precipitation events in the Weihe River Basin from 1961 to 2016[J]. Chinese Journal of Geog-

raphy, 2020, 40(5): 833-841.

[2] Zou Lei, Yu Jiangyou, Wang Feiyu, et al. The temporal and spatial evolution of extreme precipitation in the Weihe River Basin and its response to atmospheric circulation factors[J]. Arid Zone Research, 2021, 38(3): 764-774.

[3] Dai Shengpei, Luo Hongxia, Li Maofen, et al. Variation characteristics of extreme precipitation events in South China from 1959 to 2016[J/OL]. China Agricultural Resources and Regional Planning: 1-17[2021-11-30]. http://kns.cnki.net/kcms/detail/11.3513.S.20210607.1505.040.html.

[4] Du Yi, Long Kaihao, Wang Dayang, et al. Prediction of annual precipitation in Anhui province based on machine learning method[J]. Hydropower Energy Science, 2020, 38(7): 5-7, 41.

[5] Luo Zhiwen, Wang Xiaojun, Liu Mengyang, et al. Temporal and spatial characteristics of extreme precipitation in Shaanxi Province based on regional linear moment method[J]. Arid Zone Research, 2021, 38(5): 1295-1305.

[6] Zhao Yifei, Zou Xinqing, Xu Xinwanghao. Extreme precipitation events in the Pearl River Basin and its relationship with atmospheric circulation[J]. Chinese Journal of Ecology, 2014, 33(9): 2528-2537.

[7] Chen Xingren, Yang Yue, He Jianan, et al. Analysis on the characteristics of temporal and spatial changes of continuous extreme precipitation in China and its circulation factors in the past 60 years[J]. Resources and Environment in the Yangtze Basin, 2020, 29(9): 2068-2081.

[8] Liu Yanfei, Long Xiao, Wang Hui. Numerical simulation studies on a rainstorm in central Western Shaanxi Province[J]. Plateau Meteorology, 2015, 34(2): 378-388.

[9] Bai Aijuan, Shi Neng. East Asian winter/summer monsoon intensity index and its relationship with precipitation change in Shaanxi Province[J]. Journal of Nanjing Institute of Meteorology, 2004, 37(4): 519-526.

[10] Liu Changxin, Zhang Hailing, Wu Jing. Assessment of the impact of extreme precipitation in China based on SSPs scenarios[J]. Environmental Protection, 2021, 49(8): 29-34.

[11] Zhou Yaman, Liu Jing, Zhao Yong, et al. Study on the relationship between spring tropical sea temperature and extreme summer precipitation in northern Xinjiang[J]. Journal of Glaciology and Geocryology, 2021, 43(4): 1166-1178.

[12] Ma Mengyang, Han Yuping, Wang Qingming, et al. The temporal and spatial variation of extreme precipitation in the Haihe River Basin and its relationship with atmospheric circulation[J]. Hydropower Energy Science, 2019, 37(6): 1-4.

[13] Zhang Chong, Zhao Jingbo. The impact of El Niño/La Nina event on the climate of Shaanxi[J]. Journal of Shaanxi Normal University(Natural Science Edition), 2010, 38(5): 98-104.

[14] Dou Ruiyin, Yan Junping. Responses of drought and flood disasters in Guanzhong area from 1960 to 2010 to climate change[J]. Journal of Hunan Agricultural University (Natural Science Edition), 2012, 38(5): 542-547.

[15] Liu Yan, Li Jing, Qin Keyu, et al. Scenario-based prediction and change analysis of land use and ecosystem services in the Guanzhong Plain[J]. Journal of Shaanxi Normal University(Natural Science Edition), 2018, 46(2): 95-103.

[16] Zhou B, Xu Y, Wu J, et al. Changes in temperature and precipitation extreme indices over China: Analysis of a high resolution grid dataset[J]. International Journal of Climatology, 2016, 36(3): 1051-1066.

[17] Shao Jun. Hydrological multi-scale correlation analysis based on cross wavelet transform[J]. Journal of Hydroelectric Engineering, 2013, 32(2): 22-26.

[18] Zhang Jing, Zhang Ke, Wang Sheng, et al. Analysis of the temporal and spatial changes of extreme precipitation in the source area of the Three Rivers in Shaanxi, Gansu and Ningxia from 1971 to 2017[J]. Journal of Hohai University (Natural Science Edition), 2021, 49(3): 288-294.

[19] Wang Gang, Yan Denghua, Zhang Dongdong, et al. Analysis on the trend of extreme temperature and precipitation in the Haihe River Basin from 1961 to 2010[J]. South North Water Diversion and Water Conservancy Science and Technology, 2014, 12(1): 1-6.

[20] Khaled H Hamed. Trend detection in hydrologic data: The Mann Kendall trend test under the scaling hypothesis[J]. Journal of Hydrology, 2008, 349(3-4): 350-363.

[21] Grinsted A, Moore J C, Jevrejeva S. Application of the cross wavelet transform and wavelet coherence to geophysical time series[J]. Nonlinear Processes in Geophysics, 2004, 11(5/6): 561-566.

[22] Lachaux J P, Lutz A, Rudrauf D, et al. Estimating the time of coherence between single trial brain signals: An introduction to wavelet coherence[J]. Neurophysiologie Clinique/Clinical Neurophysiology, 2002, 32(3): 157-174.

Figures

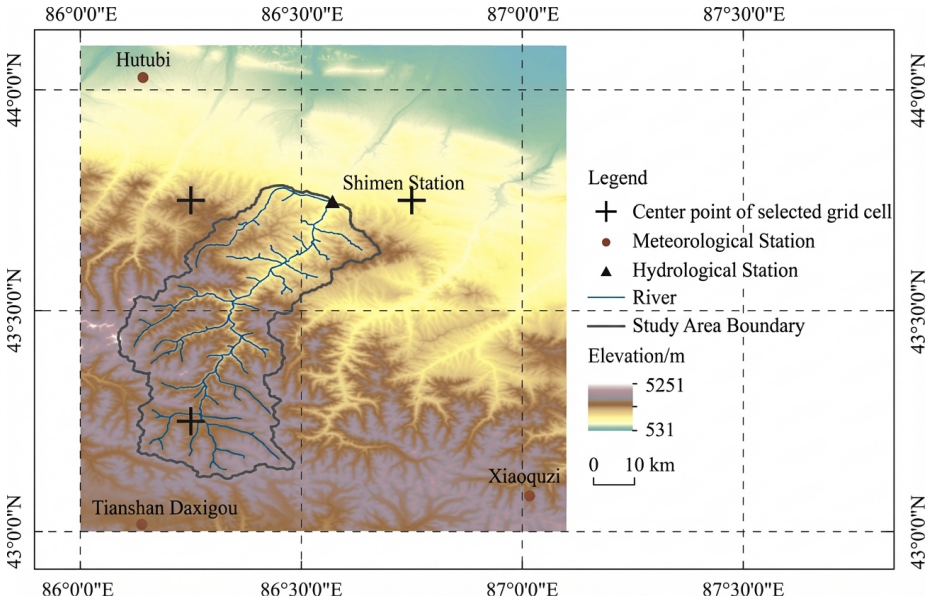

Figure 1: Figure 1

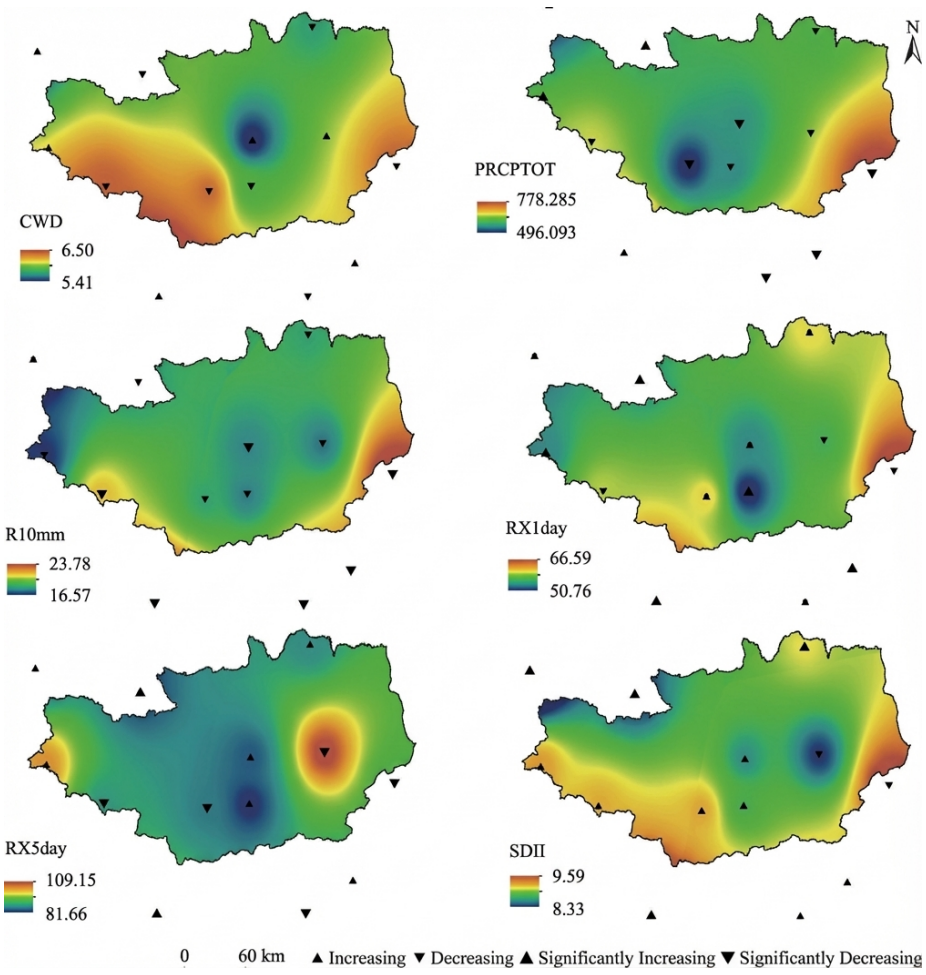

Figure 2: Figure 3